DOI: 10.1002/ejoc.200700778

Strength vs. Accessibility: Unraveling the Patterns of Self-Recognition in a Conformationally Locked Amino Alcohol

Goverdhan Mehta,*[a] Saikat Sen,[a] Tayur N. Guru Row,[b] Deepak Chopra,[b] and Sayani Chattopadhyay[a]

Keywords: Amino alcohol / Self-assembly / Hydrogen bonding / Experimental charge density

Unlike the self-assembly of aminols studied till date, that of the conformationally locked, *trans*-amino alcohol under study is unique in having the amino protons serving as mere spectators in the crystal packing. The principal non-covalent interactions, holding the molecules in the crystal lattice, are O–H···N hydrogen bonds, and the rarely encountered π-π stacking interactions between the isolated double bonds. Experimental charge density analyses have been carried out on the amino alcohol not only to characterize the non-covalent interactions existing in the supramolecular assembly in terms of the topological features of electron density at their bond critical points, but also to elucidate the apparent presence of the "spectator" amino hydrogen atoms beyond the criteria of mere geometry.

Introduction

As a "supramolecule *par excellence*", a crystal strives in its formation to optimize the various non-covalent interactions that build up the lattice through a precise matching of the functionalities.[1] This generality is embodied not only in the principle of maximization of hydrogen bonding, but also in the often applied H-bond rule that "all good proton donors and acceptors are used in hydrogen bonding".[2,3] Indeed, crystal structures, in which potential hydrogen-bond donors do not involve themselves at all in either strong or weak H-bonding, are so rare that any aberration is ascribed in most cases to an inaccurate determination of the hydrogen atom positions in the crystal lattice from the available X-ray diffraction data. A notable exception to this widely accepted crystallagraphic lore is the crystal structure of alloxan, which evidently constitutes a topic of much discussion even to this date.[4] Against this background, we describe herein an unique observation of true spectator amino protons[5] in a conformationally locked amino alcohol **1** that assembles in the crystal lattice solely through O–H···N hydrogen bonds and weaker π-π stacking interactions. The present study was a natural extension of our ongoing investigations into the effect of conformational locking on supramolecular assemblies, held primarily through strong hydrogen bonds (such as O–H···O),[6] and was further motivated by the recent investigations into the supramolecular assemblies of crystalline aminols.[7–9]

Through their systematic studies into the crystal structures of linear diphenol–diamine complexes, aminophenols and aminols, such as ethanolamine, Ermer and Erling had demonstrated that complementarity of hydrogen bonding capabilities of OH and NH_2 groups manifests itself in the saturation of H-bonding potential of the two functionalities with tetrahedral environment about the O and N atoms (Figure 1).[7]

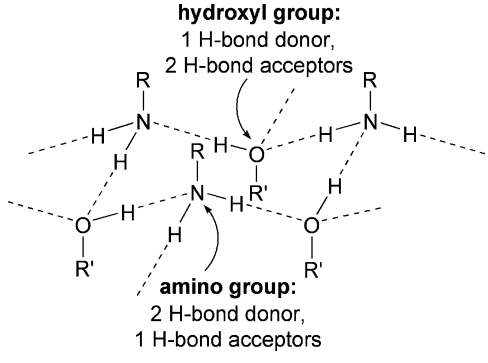

Figure 1. Complementarity of O–H···N and N–H···O hydrogen bonds in 1:1 alcohol–amine complex, leading to tetrahedral coordination around each O and N atom.

A simlar recognition between hydroxy and amino groups was observed by Hanessian and co-workers in crystalline binary complexes of diaminocyclohexanes and cyclohexanediols.[8] However, it was recently demonstrated by Desiraju and co-workers that the need to optimize herringbone interactions (interaction interference) can result in the

[a] Department of Organic Chemistry, Indian Institute of Science, Bangalore 560012, India
Fax: +91-80-23600283
E-mail: gm@orgchem.iisc.ernet.in
[b] Solid State and Structural Chemistry Unit, Indian Institute of Science,
Bangalore 560012, India
Supporting information for this article is available on the WWW under http://www.eurjoc.org or from the author.

breakdown of the foregoing H-bonding model in the supramolecular assemblies of aminophenols and that a variety of supramolecular synthons, based on O–H···N, N–H···O and N–H···π hydrogen bonding, can be identified in the crystal structures of such compounds (Figure 2).[9] The authors further ventured to extend the information gleaned from these supramolecular synthons to predict the crystal structures of a number of aminol molecules. Evidently, the concepts and models of crystal packing in aminols, put forth in the several studies referred to above, formed the starting point of our investigations into preferred mode of self-assembly in a conformationally locked amino alcohol such as **1**.

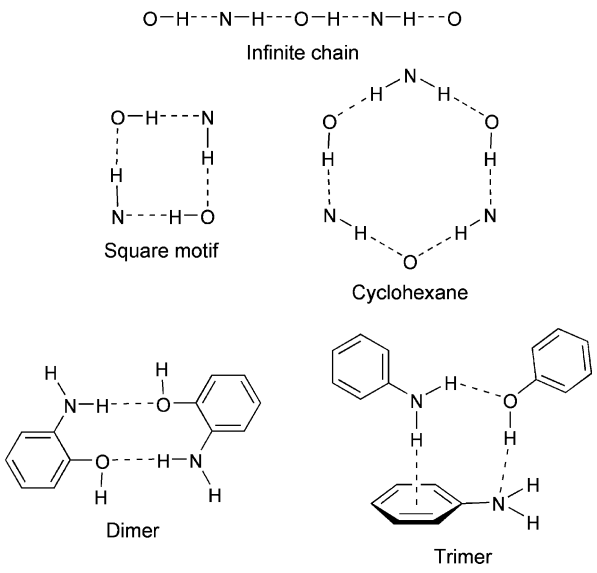

Figure 2. A selection of the supramolecular synthons identified in a recent study of the crystal structures of aminols.[9]

Results and Discussion

(a) Synthesis and Preliminary Crystallographic Studies

The amino alcohol **1** was conveniently synthesized through LAH reduction of the azide functionality in **3**, which in turn was obtained from the epoxide **2** via NaN_3/$LiClO_4$-mediated ring opening (Scheme 1).

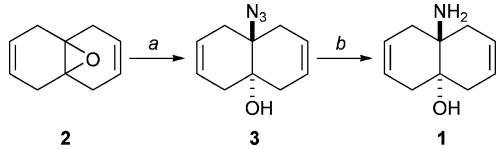

Scheme 1. *Reagents and conditions*: (a) NaN_3, $LiClO_4$, MeCN, 80 °C, 21 h, 92%; (b) $LiAlH_4$, 0 °C → r.t., THF, 4 h, 95%.

Single crystals of **1** were grown at ca. 5 °C by slow solvent evaporation of their dilute solutions in 2:1:1 petroleum ether/dichloromethane/triethylamine. Single-crystal X-ray diffraction data, collected initially at 291 K, revealed that the amino alcohol **1** (see Figure 3 for the ORTEP diagram of **1**, plotted from the data collected at 90 K) packs in the centrosymmetric monoclinic space group $P2_1/c$ (Z = 4), with O–H···N H-bonds following the c glide symmetry to link molecules of **1** into chains along the c axis. Offset parallel π-π stacking interactions between the olefinic bonds connect the molecular chains translated along the a axis (see Figure 4 for the molecular packing diagram of **1** as discerned from the crystal data collected later at 90 K).

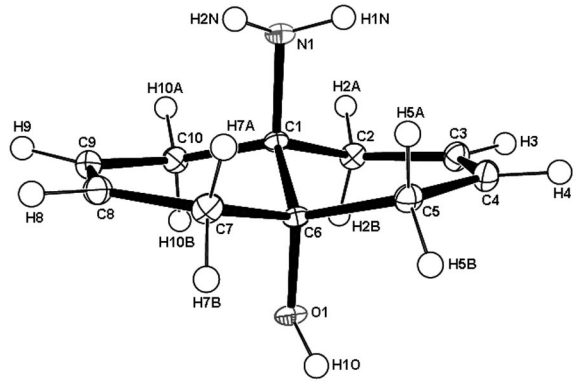

Figure 3. ORTEP diagram of the amino alcohol **1**, with atom numbering scheme for the asymmetric unit. Displacement ellipsoids (90 K) have been drawn at 50% probability level and H atoms are shown as small spheres of arbitary radii.

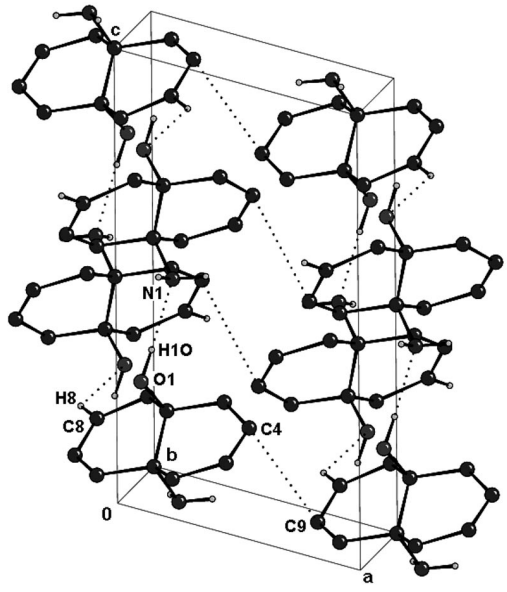

Figure 4. Molecular packing of the amino alcohol **1** as observed at 90 K. Non-interacting H-atoms bonded to C atoms have been omitted for clarity. The C–H···O H-bond, seen here, is far too weak to be consequential in the supramolecular assembly of **1** at 291.

However, barring possible intramolecular N–H···H–C and N–H···π bonds, *the amino protons in **1** appeared to participate in, at best, a rather weak N–H···π or no intermolecular interaction at all* (Figure 5).[10]

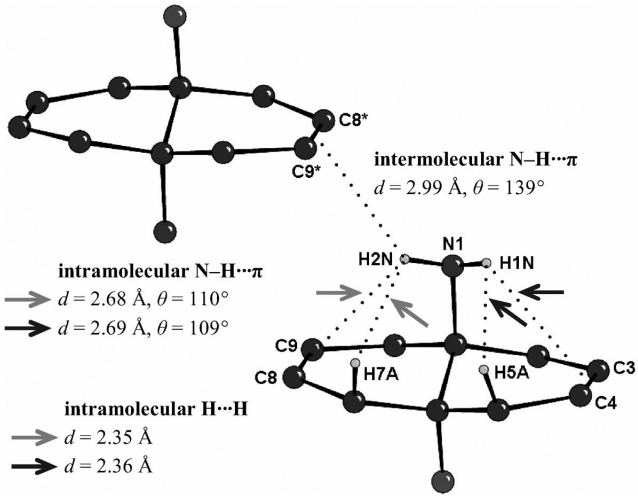

Figure 5. The interatomic and intermolecular N–H···X contacts, less than 3.00 Å, observed in the molecular packing of **1** at 291 K.

This observation was rather intriguing, as previous studies on molecular packing in aminols have shown a consistent and definitive role of the NH_2 protons in the supramolecular assembly via the formation of robust intermolecular N–H···O, N–H···N and even N–H···π hydrogen bonds.[7–9] With the intent of analyzing all possible N–H···X interactions beyond the criteria of mere geometry and elucidating the apparent presence of the "spectator" amino hydrogen atoms in the supramolecular assembly of **1**, a detailed analysis of the topological properties of the electron density (ED) in the crystal structure of **1** was sought.[11]

(b) Charge Density Analysis of the Amino Alcohol 1

A detailed analysis of the charge density distribution in crystalline **1** was carried out with the XD software package[12] by applying the Hansen–Coppens multipole formalism of atomic charges[13] on a high resolution ($[\sin\theta/\lambda]_{max}$ = 1.04 $Å^{-1}$, 98.0% overall completion) X-ray diffraction data set collected on the amino alcohol **1** at 90(2) K. The structural model of **1**, employed for the experimental determination of ED, was found to fulfil the Hirshfeld's rigid bond postulate,[14] the DMSDA along the interatomic vector for

Table 1. Differences of mean-squares displacement amplitudes (DMSDA).

Atom A	Atom B	DMSDA [10^{-4} Å^2]	Atom A	Atom B	DMSDA [10^{-4} Å^2]
O1	C6	4	C2	C3	1
C6	C5	3	C8	C9	1
C1	C10	3	C5	C4	0
N1	C1	2	C6	C1	0
C6	C7	2	C2	C1	–2
C10	C9	1	C8	C7	–4
C3	C4	1			

Table 2. Topological features of the electron density at the intramolecular bond critical points.[a]

Bond (A–B)	ρ_b [e Å^{-3}]	$\nabla^2\rho_b$ [e Å^{-5}]	R_{ij} [Å]	$d1$ [Å]	$d2$ [Å]	λ_1 [e Å^{-5}]	λ_2 [e Å^{-5}]	λ_3 [e Å^{-5}]	$\varepsilon = \lambda_1/\lambda_2 - 1$
N(1)–C(1)	1.764(13)	–15.290(54)	1.4808	0.8639	0.6169	–13.84	–10.57	9.11	0.31
N(1)–H(1N)	2.356(39)	–28.903(187)	1.0091	0.7289	0.2802	–29.38	–27.75	28.23	0.06
N(1)–H(2N)	2.439(40)	–29.444(175)	1.0095	0.7120	0.2975	–29.48	–27.81	27.85	0.06
O(1)–C(6)	1.827(14)	–19.047(63)	1.4294	0.8700	0.5594	–14.53	–11.77	7.26	0.23
O(1)–H(1O)	2.641(44)	–37.385(236)	0.9674	0.7124	0.2550	–38.80	–35.82	37.23	0.08
C(1)–C(10)	1.860(12)	–20.572(38)	1.5345	0.7857	0.7489	–14.62	–12.93	6.98	0.13
C(2)–C(1)	1.779(12)	–16.846(36)	1.5355	0.7455	0.7900	–12.88	–11.59	7.62	0.11
C(2)–C(3)	1.870(12)	–19.617(36)	1.5039	0.7361	0.7677	–13.89	–12.67	6.95	0.10
C(2)–H(2A)	1.774(27)	–18.141(69)	1.0930	0.6624	0.4306	–14.89	–14.49	11.24	0.03
C(2)–H(2B)	1.813(29)	–18.273(85)	1.0925	0.7050	0.3874	–16.11	–15.37	13.20	0.05
C(3)–C(4)	2.225(19)	–21.017(75)	1.3398	0.7149	0.6249	–15.52	–10.86	5.36	0.43
C(3)–H(3)	1.825(32)	–17.500(92)	1.0772	0.6932	0.3840	–16.15	–14.95	13.60	0.08
C(4)–H(4)	1.922(31)	–22.119(95)	1.0771	0.6847	0.3924	–18.48	–16.97	13.33	0.09
C(5)–C(4)	1.776(14)	–15.284(47)	1.5043	0.7395	0.7648	–11.90	–11.73	8.35	0.01
C(5)–H(5A)	1.779(29)	–16.624(86)	1.0921	0.7026	0.3896	–15.62	–14.93	13.93	0.05
C(5)–H(5B)	1.770(26)	–18.359(70)	1.0927	0.6664	0.4262	–15.35	–14.46	11.45	0.06
C(6)–C(1)	1.649(12)	–14.303(38)	1.5520	0.7743	0.7776	–11.32	–10.53	7.55	0.07
C(6)–C(5)	1.845(12)	–20.071(39)	1.5433	0.7947	0.7486	–14.20	–12.78	6.91	0.11
C(6)–C(7)	1.826(11)	–18.339(35)	1.5431	0.7721	0.7710	–13.36	–12.29	7.31	0.09
C(7)–H(7A)	1.765(28)	–16.863(86)	1.0922	0.7096	0.3826	–15.74	–15.07	13.95	0.04
C(7)–H(7B)	1.783(28)	–18.400(72)	1.0922	0.6603	0.4319	–15.22	–14.49	11.31	0.05
C(8)–C(7)	1.871(15)	–19.668(47)	1.5048	0.7516	0.7533	–14.34	–13.03	7.70	0.10
C(8)–C(9)	2.222(19)	–20.883(70)	1.3410	0.6361	0.7049	–15.69	–10.77	5.58	0.46
C(8)–H(8)	1.874(30)	–18.661(94)	1.0771	0.6930	0.3841	–16.91	–16.41	14.66	0.03
C(9)–H(9)	1.879(29)	–20.781(74)	1.0811	0.6609	0.4202	–16.47	–15.54	11.23	0.06
C(10)–C(9)	1.828(11)	–17.229(35)	1.5044	0.7420	0.7624	–12.80	–11.85	7.43	0.08
C(10)–H(10A)	1.804(28)	–19.459(70)	1.0929	0.6566	0.4363	–15.56	–14.60	10.71	0.07
C(10)–H(10B)	1.837(31)	–18.186(92)	1.0921	0.7081	0.3840	–16.58	–15.46	13.86	0.07

[a] Definitions: ρ_b, electron density at the bond critical point; $\nabla^2\rho_b$, Laplacian at the bond critical point; R_{ij}, bond length; $d1$, bond path from the nucleus A to the critical point; $d2$, bond path from the critical point to the nucleus B; λ_1, λ_2, λ_3, principal components of $\nabla^2\rho_b$; ε, bond ellipticity.

any pair of covalently bonded non-H atoms in **1** not exceeding 4×10^{-4} Å^2 (Table 1). The quality of the fit obtained in the multipole refinement was judged from the residual ED, evaluated at the end of the refinement protocol. The highest peak and deepest hole in the residual ED map of **1** were 0.208 and –0.194 e Å^{-3}, respectively, thereby attesting to the success of the ED model (Figure 6). Topological features of the static ED, calculated at the 28 intramolecular bond critical points (BCPs),[15] were too along the lines of those expected for the respective covalent bonds in the amino alcohol **1** (Table 2, Figure 7 and Figure 8).

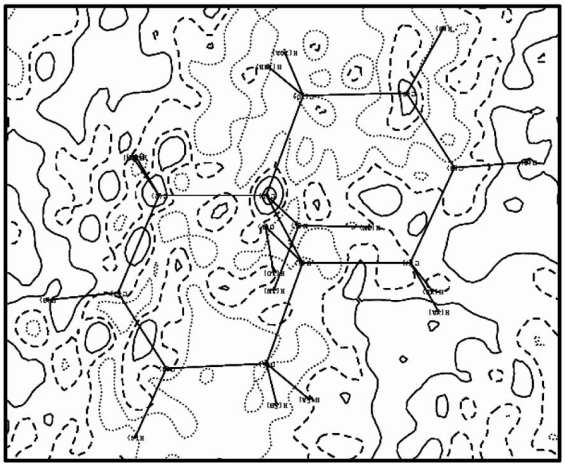

Figure 6. Residual electron density in the molecular plane defined by C1, C2 and C3. Solid lines indicate positive contours, dotted lines negative contours and dashed lines zero contours. The first positive contour is at 0.05 e Å^{-3} and the contour levels are at 0.10 e Å^{-3} intervals. The first negative contour is at –0.05 e Å^{-3} and the contour levels are at –0.10 e Å^{-3} intervals. Owing to the puckered conformation of the bicyclic ring system, the entire molecule has been represented for the sake of clarity.

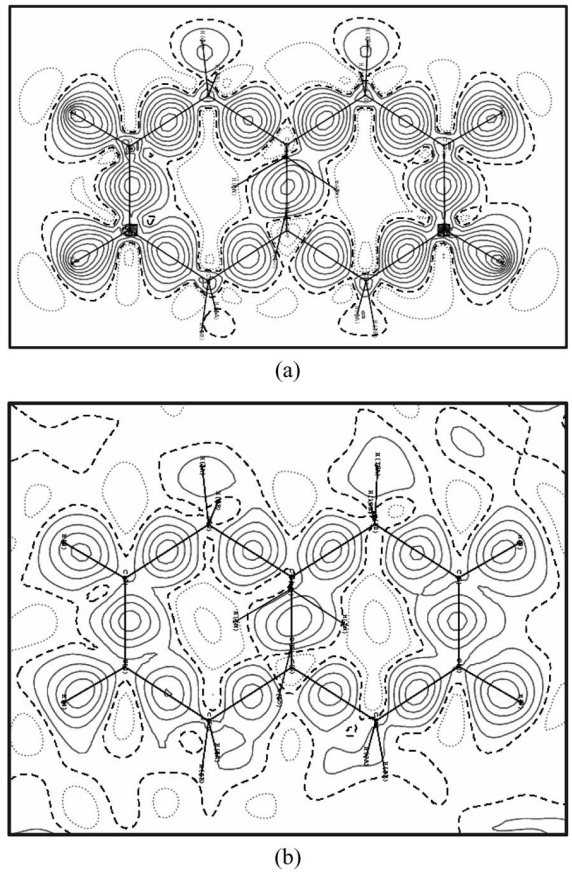

Figure 7. (a) Static deformation density and (b) dynamic deformation density maps in molecular planes defined by C3, C4 and C8. Solid lines indicate positive contours, dotted lines negative contours and broken lines zero contours. The first positive and negative contours are at 0.05 and –0.05 e Å^{-3}, respectively; the contour levels are at 0.10 and –0.10 e Å^{-3} intervals, respectively. Owing to the puckered conformation of the bicyclic ring system, the entire molecule has been represented for the sake of clarity.

In the subsequent step, all possible interatomic contacts in **1**, within the distance range r = 1.70–3.80 Å (r_{max} was kept at 3.00 Å for the intramolecular contacts) and particularly those involving the amino protons, were screened for the existence of a BCP between the donor and acceptor atoms via a bond path. In addition, interatomic contacts, involving a donor H atom and satisfying the foregoing first of the eight conditions proposed as benchmarks of a H-bond by Koch and Popelier, were examined for their compliance with the latter.[16] No BCP with the attendant topological features of an N–H···X interaction was observed in case of the interatomic contacts involving the NH_2 protons (Figure 9).[17] As observed earlier, the prominent O–H···N hydrogen bonds and well-defined π-π stacking interactions were found to be the only definitive packing forces in supramolecular assembly of **1** (Figure 10, Table 3). A rather weak C–H···O H-bond, attendant with the largest contraction of the crystal lattice along the *b* axis at 90 K, was also perceived as following the 2_1 symmetry and linking the O–H···N H-bonded molecular chains along the (010) direction (Figure 4, Table 3).

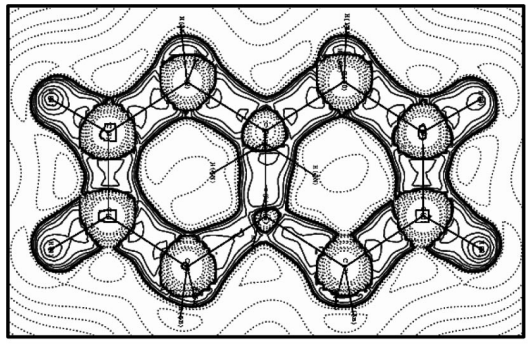

Figure 8. Laplacian distribution map in molecular planes defined by C3, C4 and C8. Contours are drawn at logarithmic intervals in $\nabla^2\rho_b$, e Å^{-5}. Solid lines indicate positive contours and dotted lines negative contours. Owing to the puckered conformation of the bicyclic ring system, the entire molecule has been represented for the sake of clarity.

It appeared reasonable to ask at this juncture as to whether the particular spatial disposition of the spectator amino protons, observed in the crystal structure of **1**, represents a highly favored ground state conformation of the

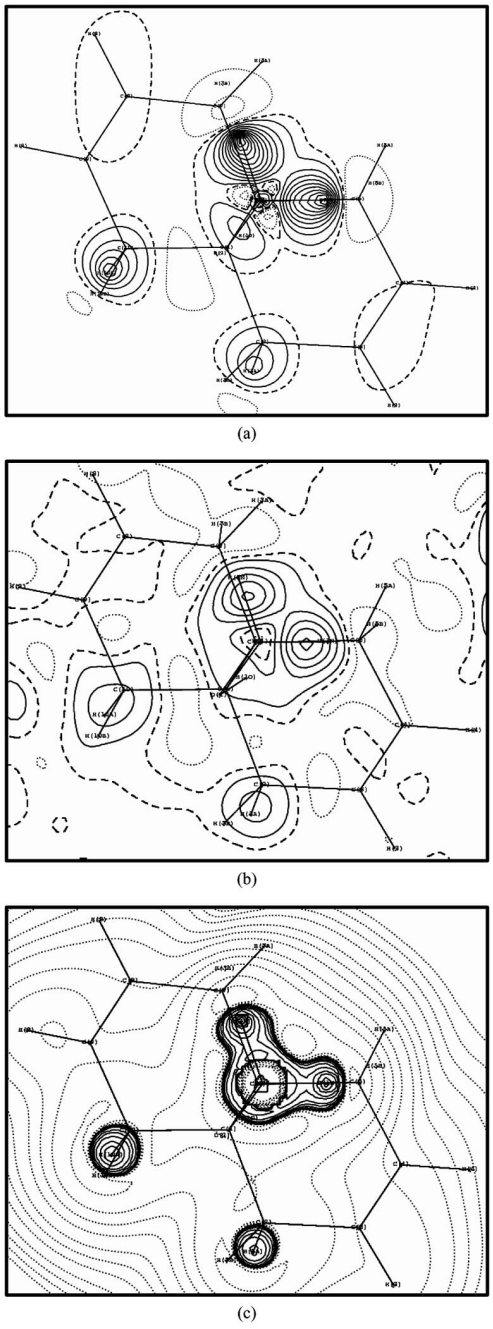

Figure 9. (a) Static deformation density and (b) dynamic deformation density maps in the molecular plane defined by N1, H1N, H2N. Solid lines indicate positive contours, dotted lines negative contours and broken lines zero contours. The first positive and negative contours are at 0.05 and –0.05 e Å^{-3}, respectively; the contour levels are at 0.10 and –0.10 e Å^{-3} intervals, respectively. (c) Laplacian distribution map in molecular planes defined by N1, H1N, H2N. Contours are drawn at logarithmic intervals in $\nabla^2\rho_b$, e Å^{-5}. Solid lines indicate positive contours and dotted lines negative contours. Owing to the puckered conformation of the bicyclic ring system, the entire molecule has been represented in all the maps for the sake of clarity.

amino alcohol. How would it correlate among the low energy gas phase conformations computed for the amino alcohol **1**?

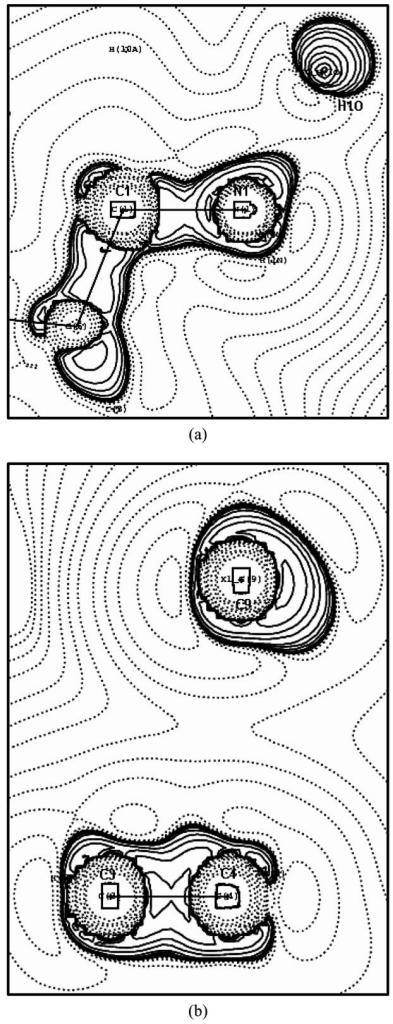

Figure 10. Laplacian distribution maps in planes defined by the (a) C1–N1···H1O hydrogen bond, and (b) C3–C4···C9 π-π stacking interactions. Contours are drawn at logarithmic intervals in $\nabla^2\rho_b$, e Å^{-5}. Solid lines indicate positive contours and dotted lines negative contours.

(c) Quantum Mechanical Calculations

All theoretical calculations pertaining to the conformational analysis of the amino alcohol **1** were performed using the software GAUSSIAN 98.[20] DFT based relaxed potential energy surface (PES) scan studies on **1** were performed at the B3LYP/6-311++G(d,p) level, with geometry optimization and single point energy calculations at each point on a rectangular grid involving the torsion angles, H1N–N1–C1–C6 and H1O–O1–C6–C1, each increased 6 times from 0° by 60°. Among the various conformations of the amino alcohol **1** thus identified in the PES scan, four conformations, **A**, **B**, **C** and **D** (Figure 11), had distinctly lower energies than the rest and were therefore chosen for a full geometrical optimization (followed by calculation of the IR frequencies in the final optimized structure) at the B3LYP/6-311++G(3df,3pd) (Figure 9). Absence of any imaginary vibrational frequency at the stationary point, computed by the optimization routine, indicated that a molecular conformation corresponding to a true energy minimum has been obtained.

Table 3. Intermolecular bond critical points and parameters characterizing the interactions.[a]

Bond path	N(1)···H(1O)	C(4)···C(9)	O(1)···H(8)
Symmetry operation	x, 1/2 –y, 1/2 + z	x, y, z	–x, 1/2 + y, 1/2 –z
R [Å]	1.9995	3.7648	2.6545
$\Delta r_D - \Delta r_A$ [Å]	0.3699	–0.1326	0.1869
$\Delta r_D + \Delta r_A$ [Å]	0.7505	–0.3648	0.0655
ρ_b [e Å^{-3}]	0.104	0.028	0.035
$\nabla^2\rho_b$ [e Å^{-5}]	3.755	0.224	0.589
λ_1 [e Å^{-5}]	–0.70	–0.10	–0.13
λ_2 [e Å^{-5}]	–0.43	–0.04	–0.12
λ_3 [e Å^{-5}]	4.89	0.36	0.84
G (r_{CP}) [kJ mol^{-1} bohr^{-3}]	75.38	4.88	11.87
V (r_{CP}) [k J mol^{-1} bohr^{-3}]	–48.48	–9.69	–23.58

[a] Definitions: R, total bond path length; $\Delta r_X = r_X^o - r_X$, where r_X^o, r_X are the nonbonded and bond critical point radii; ρ_b, electron density at the bond critical point; $\nabla^2\rho_b$, Laplacian at the bond critical point; λ_1, λ_2, λ_3, principal components of $\nabla^2\rho_b$; G (r_{CP}), local electronic kinetic energy at bond critical point = $(3/10)(3\pi2)^{2/3}(\rho_b)^{5/3} + (1/6)\nabla^2\rho_b$ (in a.u.);[18] V (r_{CP}), local potential energy at bond critical point = $(1/4)\nabla^2\rho_b - 2G$ (r_{CP}) (in a.u.).[19]

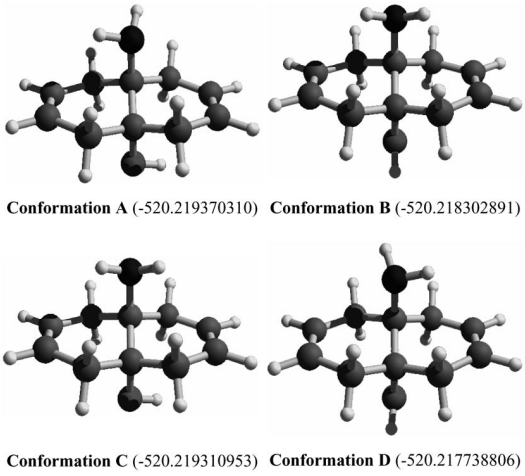

Figure 11. Four lowest energy conformations of the amino alcohol **1**. The quantity in parenthesis refers to energy (in Hartrees) of the optimized geometry, as calculated at B3LYP/6-311++G(3df,3pd) level.

Interestingly, the molecular conformation **A**, not **B**, was found to represent the global minima on the PES of **1** (Figure 11). In striking contrast to **B**, a conformation akin to that observed in the crystal structure of **1**, it is the hydroxy, instead of the amino, proton in **A** that point towards the interior of the molecule. Hence, going by the precedence of the crystal packing in **1**, conformation **A** presents a spatial arrangement of NH_2 and OH hydrogen atoms more suited for N–H···O than O–H···N H-bonding (Figure 11).

However, geometry optimization of N–H···O and O–H···N H-bonded dimers of **A** and **B**, respectively, employing both ab initio (HF/6-31G*) and DFT (B3LYP/6-31G*) methods, revealed that the H-bonded dimers of **A** are less stable than those of **B** by an amount of about 14 kJ mol^{-1} (Figure 12).[21] Hence, given the fact that the difference in energy between **A** and **B** was found to be smaller than the thermal energy of the molecules at the crystallization temperature, the preferred mode of self assembly of **1** through O–H···N hydrogen bonding, involving the more acidic hydroxy H-atom and the more basic amino group, can easily be accounted for. Such a H-bonding pattern automatically relegates the protons of the tertiary amino group to the interior of the conformationally constrained carbocyclic scaffold in **1**, making them far less accessible than peripheral C=C bonds. The consequence is quite apparent in the well-defined and rather less encountered π-π stacking interactions between the isolated double bonds in the crystal structure of **1**.

(d) Crystallographic Studies on the Amino Alcohol 4, a Perhydro Variant of 1

Presence of the distinct π-π stacking interactions in the crystal structure of **1** prompted us to investigate the solid state supramolecular assembly of the amino alcohol **4** (Figure 13), which was conveniently synthesized from the unsaturated azido alcohol **3** via catalytic hydrogenation. After several trials, crystals of **4**, suitable for single-crystal X-ray crystallography, was obtained by slow evaporation of its solution in 2:1:1 petroleum ether/CH_2Cl_2/Et_3N at ca. 5 °C. However, these crystals were observed to lose crystallinity quite rapidly on exposure to air even at low temperature (this precluded the possibility of collecting low temperature data), so that the X-ray data was collected as expeditiously as possible on a good quality crystal of **4**, mounted inside a Lindeman capillary.

Crystals of the amino alcohol **4** (Figure 13) exhibited isostructurality to those of its unsaturated sibling **1**, and belonged to the centrosymmetric monoclinic space group $P2_1/c$ (Z = 4). The packing in crystalline **4** followed an identical trend as the archetypical **1** with O–H···N H-bonding linking the molecules as chains parallel to the c axis (Figure 14 and Figure 15). These molecular chains are in turn connected parallel to the b axis by weak C–H···O interactions, following the symmetry of the 2_1 screw (Table 4, Figure 14). In both instances of **1** and **4**, the amino protons, buried within the molecular bulk, were left as mere spectators in the supramolecular assembly, with the weaker yet more accessible interactions (π-π stacking for **1** and C–H···O for **4**) exhibiting their presence in the crystal packing.

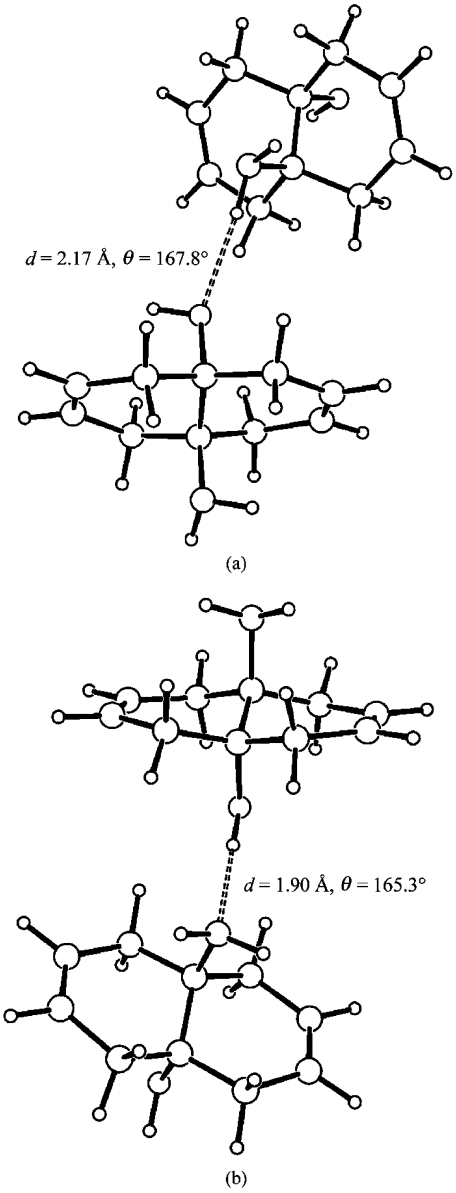

Figure 12. Optimized geometry of (a) N–H···O and (b) O–H···N H-bonded molecular dimers constructed from conformations A and B, respectively. Calculated energy (in Hartrees): (a) for the N–H···O H-bonded molecular dimer: –1033.37563678 (HF/6-31G*), –1040.05420174 (B3LYP/6-31G*); (b) for the O–H···N H-bonded molecular dimer: –1033.37919987 (HF/6-31G*); –1040.05948653 (B3LYP/6-31G*).

Conclusions

As a novel addition to the existing information on the supramolecular chemistry of amino alcohols, the crystal structures of **1** and **4** provide a new perspective to the understanding of molecular packing in this class of compounds. Indeed, when compared to the models of hydrogen bonding proposed for aminols to date, the self-assembly of amino alcohols **1** and **4** presents an extreme case, in which conformational locking ("interference") completely sequesters an otherwise dominant H-bond donor. This observation was elucidated beyond the criteria of mere geometry in

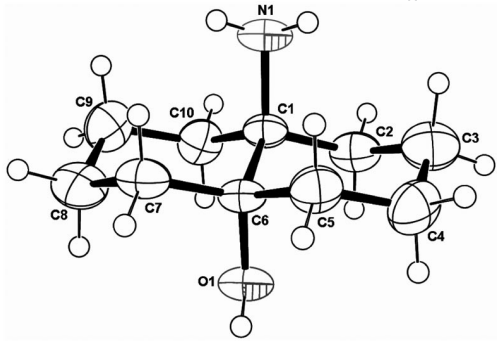

Figure 13. ORTEP diagram of the amino alcohol **4**, with atom numbering scheme for the asymmetric unit. Displacement ellipsoids (291 K) have been drawn at 50% probability level and H atoms are shown as small spheres of arbitary radii.

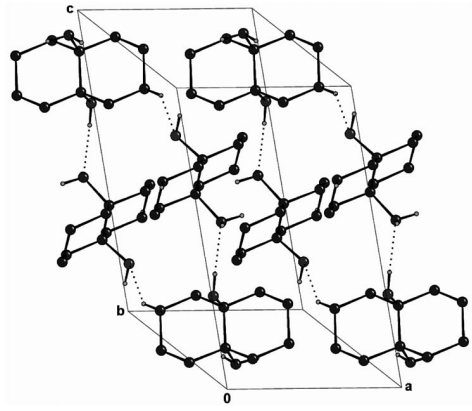

Figure 14. Molecular packing of the amino alcohol **4** as observed at 291 K. Non-interacting H-atoms bonded to C atoms have been omitted for clarity.

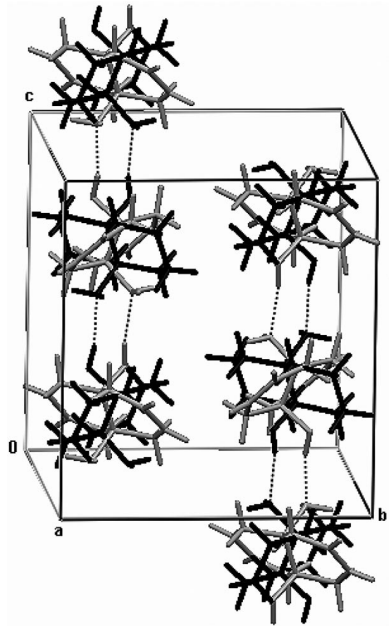

Figure 15. Comparison of the molecular packing (291 K) via O–H···N H-bonding in the amino alcohols **1** (dark gray) and **4** (black). The unit cells have been colored following the color code of the respective molecules.

Table 4. Hydrogen bond geometry (Å,°) in the amino alcohol **4**.

D–H···A[a]	D–H	H···A	D···A	D–H···A
O1–H1O···N1^{i}	0.84(3)	2.06(3)	2.889(3)	169(3)
C8–H8A···O1^{ii}	0.97	2.66	3.520(4)	148

[a] Symmetry codes: (i) x, 3/2 $-y$, $-1/2 + z$; (ii) $2 - x$, $1/2 + y$, $1/2 - z$.

the crystal structure of **1** through experimental charge density analysis, which confirmed the non-involvement of the amino H-atoms in any form of either intra- or intermolecular hydrogen bonds. The robustness of the O–H···N synthon, as judged from the near invariance of the molecular packing in **1** and **2**, should also be noted at this point. Taken in a wider perspective, the present study puts forward the possibility of engineering solid-state assemblies of specially crafted molecules, wherein conformational locking may be employed as a tool to disable the structural interference of an activated hydrogen-bond donor, while retaining its role either as a H-bond acceptor or an indispensable moiety necessary for the desired functional property of the solid.

Experimental Section

Syntheses of the Amino Alcohols 1 and 4: Infrared spectra were recorded on JASCO FT-IR 410. ^{1}H NMR and ^{13}C NMR spectra were recorded on JEOL JNM-LA 300 spectrometer. Chemical shifts are reported with respect to tetramethylsilane (Me_4Si) as the internal standard (for ^{1}H NMR) and the central line (δ = 77.0 ppm) of $CDCl_3$ (for ^{13}C NMR). The chemical shifts are expressed in parts per million (δ) downfield from Me_4Si. The standard abbreviations s, d, t, q and m refer to singlet, doublet, triplet, quartet and multiplet, respectively. Coupling constant (J), whenever discernible, have been reported in Hz. Both Low Resolution Mass Spectra (LRMS) and High Resolution Mass Spectra (HRMS) were recorded on a Q-TOF Micromass mass spectrometer. Reactions were monitored by thin-layer chromatography (tlc), which was performed either on (10 × 5 cm) glass plates or on microscopic slides, coated with Acme's silca gel G, containing 13% calcium sulfate as a binder. Visualization of the spots on the tlc plates was achieved either by exposure to iodine vapor or using UV radiation or by spraying with either ethanolic vanillin or 30% methanol/sulfuric acid solution and heating the plates at 120 °C. Commercial Acme's silica gel (100–200 mesh particle size) was used for column chromatography. Yields reported are isolated yields of materials judged homogeneous by tlc and NMR spectroscopy.

1,4,5,8-Tetrahydro-4a,8a-epoxynaphthalene (2): Epoxide **2** was prepared from 1,4,5,8-tetrahydronaphthalene as previously reported.[6d]

***anti*-8a-Azido-1,4,4a,5,8,8a-hexahydro-4a-naphthalenol (3):** A solution of the epoxide **2** (444 mg, 3 mmol), anhydrous $LiClO_4$ (321 mg, 3 mmol) and NaN_3 (325 mg, 5 mmol) in dry acetonitrile (7 mL) was refluxed for 21 h under nitrogen atmosphere. The reaction was then quenched with minimum quantity of water, and the aqueous phase extracted with dicloromethane (3 × 10 mL). The combined organic solution was dried with anhydrous sodium sulfate, filtered and concentrated to dryness. The residue thus obtained was subjected to column chromatography over silica gel (100–200 mesh) with 15% EtOAc/hexane to obtain the azido alcohol **3** as a colorless viscous oil (527 mg, 92%). FTIR (KBr): = $\tilde{\nu}$ = 3482, 3031, 2116, 1655 cm^{-1}. ^{1}H NMR (300 MHz, $CDCl_3$): δ = 5.67 (s, 4 H), 2.48–2.10 (m, 8 H), 1.98 (s, 1 H) ppm. ^{13}C NMR (75 MHz, $CDCl_3$): δ = 124.3 (2 C), 123.3 (2 C), 69.4, 62.0, 36.2 (2 C), 33.1 (2 C) ppm.

***anti*-8a-Amino-1,4,4a,5,8,8a-hexahydro-4a-naphthalenol (1):** $LiAlH_4$ (100 mg, 2.618 mmol) was added to a solution of the azido alcohol **3** (250 mg, 1.309 mmol) in sodium dried THF at 0 °C. The suspension was stirred for 4 h while allowing the reaction mixture to slowly attain the ambient temperature. The reaction was then quenched by careful addition of ethyl acetate followed by saturated sodium sulfate solution. The crystalline white precipitate of aluminium salts was filtered off and washed thoroughly with ethyl acetate. The combined organic solution was concentrated to dryness, and the residue purified rapidly by column chromatography over silica gel (100–200 mesh, pretreated with 20% Et_3N/EtOAc) with a 10:1 mixture of 50% EtOAc/hexane and Et_3N to obtain the amino alcohol **1** as a colorless crystalline solid (205 mg, 95%). The product darkens and deteriorates into a dark sticky mass upon prolonged exposure to air at room tempearture. FTIR (KBr): $\tilde{\nu}$ = 3358, 3209, 3022, 1650 cm^{-1}. ^{1}H NMR (300 MHz, $CDCl_3$): δ = 5.74–5.60 (m, 4 H), 2.39 (d, J = 16 Hz, 4 H), 2.17 (d1/2ABq, J = 17, 4 Hz, 2 H), 1.96 (d1/2ABq, J = 16, 5 Hz, 2 H) ppm. ^{13}C NMR (75 MHz, $CDCl_3$): δ = 125.1 (2 C), 123.6 (2 C), 70.9, 51.0, 37.4 (2 C), 36.2 (2 C) ppm. HRMS (ES) calcd. for $C_{10}H_{16}NO$ [M + H]$^+$: 166.1232, found 166.1232.

***anti*-8a-Aminoperhydro-4a-naphthalenol (4):** A heterogeneous mixture of the azido alcohol **3** (100 mg, 0.524 mmol) and 10% Pd-C (10 mg, 10% w/w) in dry methanol (2 mL) was stirred overnight in an atmosphere of hydrogen at 1 Torr. The reaction mixture was then filtered through a small pad of celite and washed with methanol. The combined filtrate and washings were concentrated under vacuum, and the residue subjected to column chromatography over silica gel (100–200 mesh, pretreated with 20% Et_3N/EtOAc) with a 10:1 mixture of 50% EtOAc/hexane and Et_3N to obtain the saturated amino alcohol **4** as a colorless crystalline solid (86 mg, 97%). FTIR (KBr): $\tilde{\nu}$ = 3528, 3022 cm^{-1}. ^{1}H NMR (300 MHz, $CDCl_3$): δ = 1.78–1.42 (m, 14 H), 1.22 (d, J = 11 Hz, 2 H), 1.11 (d, J = 13 Hz, 2 H) ppm. ^{13}C NMR (75 MHz, $CDCl_3$): δ = 72.8, 52.5, 35.1 (2 C), 34.1 (2 C), 20.6 (2 C), 20.5 (2 C) ppm. HRMS (ES) calcd. for $C_{10}H_{20}NO$ [M + H]$^+$: 170.1545, found 170.1542.

X-Ray Data Collection, Structure Solution and Refinement (291 K): Single crystal X-ray diffraction data was collected on a Bruker AXS SMART APEX CCD diffractometer. The X-ray generator was operated at 50 KV and 35 mA using Mo-K_α radiation. The data was collected with a ω scan width of 0.3°. A total of 606 frames per set were collected using SMART[22] in three different settings of ϕ (0°, 90° and 180°), keeping the sample to detector distance of 6.03 cm and the 2θ value fixed at –28°. The data were reduced by SAINTPLUS;[22] an empirical absorption correction was applied using the package SADABS[23] and XPREP[22] was used to determine the space group. The crystal structure was solved by direct methods using SIR92[24] and refined by full-matrix least-squares method on F^2 using SHELXL97.[25] The geometric calculations were done by PARST[26] and PLATON.[27] All hydrogen atoms were initially located in a difference Fourier map. The methine (CH) and methylene (CH_2) H atoms were then placed in geometrically idealized positions and allowed to ride on their parent atoms with C-H distances fixed at 0.93 and 0.97 Å, respectively, and U_{iso}(H) = 1.2U_{eq}(C). The positions of the H atoms of the amino and hydroxy functionalities were refined freely, along with an isotropic displacement parameter.

Crystal Data for the Amino Alcohol 1: $C_{10}H_{15}NO$, M = 165.23, monoclinic, space group $P2_1/c$, a = 6.749(2) Å, b = 11.420(4) Å, c = 12.161(4) Å, β = 105.067(5)°, V = 905.1(5) Å^3, Z = 4, $\rho_{calcd.}$ = 1.213 g cm^{-3}, $F(000)$ = 360, μ = 0.078 mm^{-1}, R = 0.0455, wR = 0.1099, GOF = 1.071 for 1429 reflections with $I > 2\sigma(I)$.

Crystal Data for the Amino Alcohol 4: $C_{10}H_{19}NO$, M = 169.26, monoclinic, space group $P2_1/c$, a = 7.071(6) Å, b = 11.425(10) Å, c = 12.245(11) Å, β = 104.42(2)°, V = 958.1(15) Å^3, Z = 4, $\rho_{calcd.}$ = 1.173 g cm^{-3}, $F(000)$ = 376, μ = 0.075 mm^{-1}, R = 0.0612, wR = 0.1460, GOF = 1.081 for 1487 reflections with $I > 2\sigma(I)$. All the relevant CIF files have been submitted to the Cambridge Crystallographic Data Centre and assigned to the corresponding depository number.

CCDC-641487 (for **1**) and -641488 (for **4**) contain the supplementary crystallographic data. These data can be obtained free of charge from The Cambridge Crystallographic Data Centre via www.ccdc.cam.ac.uk/data_request/cif.

X-ray Data Collection, Structure Solution and Spherical Atom Refinement (90 K): The high-resolution single-crystal X-ray diffraction data was collected on a Bruker AXS SMART APEX CCD diffractometer using Mo-K_α radiation (50 kV, 35 mA). During the data collection the temperature was maintained at 90(2) K with an Oxford Cryostream N_2 open-flow cryostat. A crystal of good quality and reasonable size (0.60 × 0.54 × 0.44 mm) was mounted in a Lindeman capillary and was cooled slowly from the ambient temperature to 90 K at a uniform rate of 40 K/h. The temperature of the crystal was then allowed to stabilize for 1 h; the unit-cell parameters were determined repeatedly every 15 min hereafter until the estimated standard deviations in cell dimensions did not vary beyond acceptable limits. The diffraction data was collected using SMART[22] in three batches as detailed in Table 5, keeping the crystal to detector distance fixed at 6.03 cm. In order to perform the crystal decay correction, an additional 100 frames were collected with a ω scan width of 0.3°, maintaining 2θ and ϕ at 25° and 0° respectively. This data collection strategy has been shown to provide high resolution, large redundancy and appropriate completeness in data sets.[28]

Table 5. X-ray data collection strategy at 90 K.

Run	2θ [°]	ω [°]	ϕ [°]	ω Scan width [°]	Frames	Exposure [s]
1	–25	–25	0	–0.3	606	5
2	–25	–25	90	–0.3	606	5
3	–25	–25	180	–0.3	606	5
4	–25	–25	270	–0.3	606	5
5	–50	–50	0	–0.3	606	20
6	–50	–50	90	–0.3	606	20
7	–50	–50	180	–0.3	606	20
8	–50	–50	270	–0.3	606	20
9	–75	–75	0	–0.3	606	80
10	–75	–75	90	–0.3	606	80
11	–75	–75	180	–0.3	606	80
12	–75	–75	270	–0.3	606	80

All the 7272 frames thus collected were integrated with SAINT[22] using a narrow frame integration method. Sorting, scaling, merging, and empirical correction for absorption of the set of intensities were performed with SORTAV.[29] The crystal structure of **1** was solved by direct methods using SHELXS97[25] and refined in the spherical atom approximation (based on F^2) using SHELXL97[25] included in the package WinGX. Molecular thermal ellipsoid plots and packing diagrams were generated using ORTEP32[30] and CAMERON[31], respectively. All hydrogen atoms were located from the difference Fourier map and refined freely, along with an isotropic displacement parameter.

Multipole Refinement: The aspherical atom refinement, based on F^2, was carried out using the XD package.[12] The module XDLSM, a full-matrix least-squares program, was used to carry out the multipolar refinement. Scattering factors for all atoms were derived from the Clementi and Roetti wave functions.[32] During the least-squares refinement, the function $\Sigma w\{|F_o|^2 - K|F_c|^2\}^2$ was minimized for all 6122 reflections with $I > 3\sigma(I)$. Initially only the scale factor was refined on all reflections in order to check the accuracy of the data transfer from SHELX to XD via XDINI. Hereafter, the scale factor was allowed to refine in all the successive steps of the multipole refinement. In the next step, the positional coordinates and thermal parameters of all non H-atoms was accurately determined by carring out a higher order refinement, using 2809 reflections with $0.8 < \sin\theta/\lambda < 2.0$ Å^{-1} and $I > 3\sigma(I)$. The positional coordinates and isotropic thermal parameters of the H-atoms were subsequently refined using the lower angle reflections ($0.0 < \sin\theta/\lambda < 0.8$ Å^{-1}). Owing to unavailability of neutron scattering data on the amino alcohol **1**, the positions of the hydrogen atoms in this as well as in the subsequent refinements were fixed at the average bond length values obtained from reported neutron diffraction studies.[33] The multipole populations (upto the hexadecapole level for all non-H atoms) were now allowed to refine in a stepwise manner. For all H-atoms, the multipole expansion was truncated at l_{max} = 1 (dipole, bond-directed) level. No restraints based on chemical symmetry were applied in the refinement of the multipole populations of the atoms; the molecular electro-neutrality constraint was however switched on to ensure that the unit cell remains neutral throughout all refinements. In the next step, a single refinement of the κ parameters for all non H-atoms was performed; a single κ' was then refined along with the respective κ parameter for each group of chemically distinct non H-atoms till convergence was achieved. The κ and κ' values for all H atoms were fixed at 1.2. Finally, all the multipole parameters (including

Table 6. Crystal data, structure solution and aspherical atom refinement of the amino alcohol **1**.

Cell setting, space group	monoclinic, $P2_1/c$
Unit cell dimensions	
a [Å]	6.693(5)
b [Å]	11.285(5)
c [Å]	12.087(5)
β [°]	105.421(5)
V [Å^3]	880.1(8)
Z	4
$\rho_{calcd.}$ [g cm^{-3}]	1.247
μ [mm^{-1}]	0.080
$F(000)$	360
θ Range [°], $(\sin\theta/\lambda)_{max}$ [Å^{-1}]	2.51–47.66, 1.04
Range of h, k, l	$-13 \rightarrow h \rightarrow 13$ $-23 \rightarrow k \rightarrow 22$ $-22 \rightarrow l \rightarrow 24$
Measured reflections	42375
Unique reflections	7949
Overall completeness	98%
R_{int}	0.0323
Observed reflections [$I > 3\sigma(I)$] (N_{obs})	6122
Refinement based on	F^2
$R(F^2)$	0.0524
$R_w(F^2)$	0.0504
$R(F)$	0.0255
$R_w(F)$	0.0249
Goodness of fit (S)	2.1839

the isotropic thermal parameters of H-atoms) were refined to obtain the final model of charge density distribution. The modules XDFFT and XDFOUR was used to measure the residual electron density and the dynamic deformation density, respectively. In order to obtain a quantitative picture of the electronic structure, the module XDPROP was used for topological analysis of the electron densities. Experimental details of the crystal data, structure solution and aspherical atom refinement have been given in Table 6.

Supporting Information (see also the footnote on the first page of this article): Tables providing the multipole population parameters, κ and κ' from experimental refinements, local definition axes, fractional coordinates, thermal parameters, bond lengths and bond angles; additional elucidative deformation density and Laplacian maps.

Acknowledgments

We thank the Indian Department of Science and Technology (DST) for the CCD facility at the Indian Institute of Science (IISc), and the Super Computer Research and Education Centre at IISc for the computational facilities. G. M. and T. N. G. thank the Council for Scientific and Industrial Research (CSIR) and the DST for research support and funding. D. C. thanks CSIR for the award of a senior research fellowship.

[1] J. D. Dunitz, *Pure Appl. Chem.* **1991**, *63*, 177–185.
[2] J. M. Robertson, in *Organic Crystals and Molecules*, Cornell University Press, Ithaca, New York, **1953**.
[3] M. C. Etter, *Acc. Chem. Res.* **1990**, *23*, 120–126.
[4] a) J. D. Dunitz, W. B. Schweizer, *CrystEngComm* **2007**, *9*, 266–269; b) D. S. Coombes, G. K. Nagi, S. L. Price, *Chem. Phys. Lett.* **1997**, *265*, 532–537.
[5] A Cambridge Structural Database search (CSD; Version 5.28 of November 2006)[34] was carried out on all reported crystal structures of amino alcohols, which had been refined to $R < 0.1$ and did not contain either N–H···O (restrictions: $d < 2.3$ Å, $120° < \theta < 180°$) or N–H···π (restrictions: $d < 3.0$ Å, $120° < \theta < 180°$) hydrogen bonds. Though a number of hits were generated in the search, the majority of them corresponded to single-crystal X-ray diffraction studies carried out at room temperature, and all showed the presence of potential intra/intermolecular N–H···X short contacts (i.e. $d_{H\cdots X} <$ sum of van der Waals radii). Hence, in the absence of any substantiating evidence, it was not possible to term the amino protons in these crystal structures as *true bystanders*.
[6] a) G. Mehta, S. Sen, S. S. Ramesh, *Eur. J. Org. Chem.* **2007**, 423–436; b) G. Mehta, S. Sen, *CrystEngComm* **2005**, *7*, 656–663; c) G. Mehta, S. Sen, S. S. Ramesh, *CrystEngComm* **2005**, *7*, 563–568; d) G. Mehta, S. Sen, K. Venkatesan, *CrystEngComm* **2005**, *7*, 398–401.
[7] O. Ermer, A. Eling, *J. Chem. Soc. Perkin Trans. 2* **1994**, 925–944.
[8] S. Hanessian, R. Saladino, in *Crystal Design. Structure and Function* (Ed.: G. R. Desiraju), Perspectives in Supramolecular Chemistry, Wiley, New York, **2003**, vol. 7, pp. 77–151.
[9] A. Dey, M. T. Kirchner, V. R. Vangala, G. R. Desiraju, R. Mondal, J. A. K. Howard, *J. Am. Chem. Soc.* **2005**, *127*, 10545–10559 and references cited therein.
[10] a) C. F. Matta, in *Hydrogen Bonding – New Insights* (Ed.: S. J. Grabowski), Springer, **2006**, pp. 337–376; b) D. J. Wolstenholme, T. S. Cameron, *J. Phys. Chem. B* **2006**, *110*, 8970–8978.
[11] For recent references on experimental charge density studies in organic molecules, see: a) S. Grabowsky, T. Pfeuffer, L. Chęcińska, M. Weber, W. Morgenroth, P. Luger, T. Schirmeiter, *Eur. J. Org. Chem.* **2007**, 2759–2768; b) B. Dittrich, T. Koritsanszky, A. Volkov, S. Mebs, P. Luger, *Angew. Chem. Int. Ed.* **2007**, *46*, 2935–2938; *Angew. Chem.* **2007**, *119*, 2993–2996; c) L. Chęcińska, S. I. Troyanov, S. Mebs, C. B. Hübschle, P. Luger, *Chem. Commun.* **2007**, 4003–4005; d) E. A. Zhurova, A. I. Stash, V. G. Tsirelson, V. V. Zhurov, E. V. Bartashevich, V. A. Potemkin, A. A. Pinkerton, *J. Am. Chem. Soc.* **2006**, *128*, 14728–14734; e) L. Chęcińska, S. Mebs, C. B. Huebschle, D. Foerster, W. Morgenroth, P. Luger, *Org. Biomol. Chem.* **2006**, *4*, 3242–3251; f) D. Chopra, T. S. Cameron, J. D. Ferrara, T. N. Guru Row, *J. Phys. Chem. A* **2006**, *110*, 10465–10477; g) R. Destro, R. Soave, M. Barzaghi, L. Lo Presti, *Chem. Eur. J.* **2005**, *11*, 4621–4634; h) P. Coppens, *Angew. Chem. Int. Ed.* **2005**, *44*, 6810–6811; *Angew. Chem.* **2005**, *117*, 6970–6972; i) M. Messerschmidt, S. Scheins, L. Grubert, M. Pätzel, G. Szeimies, C. Paulmann, P. Luger, *Angew. Chem. Int. Ed.* **2005**, *44*, 3925–3928; *Angew. Chem.* **2005**, *117*, 3993–3997.
[12] T. Koritsanszky, T. Richter, P. Macci, C. Gatti, S. Howard, P. R. Mallinson, L. Farrugia, Z. W. Su, N. K. Hansen, *XD, A Computer Program Package for Multipole Refinement and Analysis of Electron Densities from Diffraction Data*, Tech. Rep., Freie University of Berlin, Berlin, Germany, **2003**.
[13] N. K. Hansen, P. Coppens, *Acta Crystallogr., Sect. A* **1978**, *34*, 909–921.
[14] F. L. Hirshfeld, *Acta Crystallogr., Sect. A* **1976**, *32*, 239–244.
[15] a) R. F. W. Bader, *Atoms in Molecules: A Quantum Theory*, Oxford University Press, Oxford, UK, **1990**; b) R. F. W. Bader, *J. Phys. Chem. A* **1998**, *102*, 7314–7323.
[16] U. Koch, P. L. A. Popelier, *J. Phys. Chem.* **1995**, *99*, 9747–9754.
[17] See electronic supporting information for details.
[18] Y. A. Abramov, *Acta Crystallogr., Sect. A* **1997**, *53*, 264–272.
[19] E. Espinosa, E. Molins, C. Lecomte, *Chem. Phys. Lett.* **1998**, *285*, 170–173.
[20] M. J. Frisch, G. W. Trucks, H. B. Schlegel, G. E. Scuseria, M. A. Robb, J. R. Cheeseman, V. G. Zakrzewski, J. A. Montgomery Jr, R. E. Stratmann, J. C. Burant, S. Dapprich, J. M. Millam, A. D. Daniels, K. N. Kudin, M. C. Strain, O. Farkas, J. Tomasi, V. Barone, M. Cossi, R. Cammi, B. Mennucci, C. Pomelli, C. Adamo, S. Clifford, J. Ochterski, G. A. Petersson, P. Y. Ayala, Q. Cui, K. Morokuma, N. Rega, P. Salvador, J. J. Dannenberg, D. K. Malick, A. D. Rabuck, K. Raghavachari, J. B. Foresman, J. Cioslowski, J. V. Ortiz, A. G. Baboul, B. B. Stefanov, G. Liu, A. Liashenko, P. Piskorz, I. Komaromi, R. Gomperts, R. L. Martin, D. J. Fox, T. Keith, M. A. Al-Laham, C. Y. Peng, A. Nanayakkara, M. Challacombe, P. M. W. Gill, B. Johnson, W. Chen, M. W. Wong, J. L. Andres, C. Gonzalez, M. Head-Gordon, E. S. Replogle, J. A. Pople, *Gaussian 98*, Revision A.11.3, Gaussian, Inc., Pittsburgh PA, **2002**.
[21] The corresponding energies of conformations **A** and **B**, calculated at B3LYP/6-31G* level, are –520.046806214 Hartrees and –520.045609989 Hartrees, respectively, so that $\Delta E = E_A - E_B \approx 3.14$ kJ mol^{-1}.
[22] Bruker. *SMART* (Version 6.028), *SAINT* (Version 6.02), *XPREP*. Bruker AXS Inc., Madison, Wisconsin, USA, **1998**.
[23] G. M. Sheldrick, *SADABS*, University of Göttingen, Germany, **1996**.
[24] A. Altomare, G. Cascarano, C. Giacovazzo, A. Guagliardi, M. C. Burla, G. Polidori, M. Camalli, *J. Appl. Crystallogr.* **1994**, *27*, 435.
[25] G. M. Sheldrick, *SHELXS97* and *SHELXL97*, University of Göttingen, Germany, **1997**.
[26] M. Nardelli, *J. Appl. Crystallogr.* **1995**, *28*, 659.
[27] A. L. Spek, *J. Appl. Crystallogr.* **2003**, *36*, 7–13.
[28] P. Munshi, T. N. Guru Row, *Acta Crystallogr., Sect. B* **2002**, *58*, 1011–1017.
[29] a) R. H. Blessing, *J. Appl. Crystallogr.* **1997**, *30*, 421–426; b) R. H. Blessing, *Acta Crystallogr., Sect. A* **1995**, *51*, 33–38.
[30] L. J. Farrugia, *J. Appl. Crystallogr.* **1993**, *32*, 837–838.
[31] D. M. Watkin, L. Pearce, C. K. Prout, *CAMERON – A Molecular Graphics Package*, Chemical Crystallography Laboratory, University of Oxford, **1993**.

[32] E. Clementi, C. Roetti, *Atomic Data and Nuclear Data Tables*, **1974**, *14*, 177–478.
[33] F. H. Allen, O. Kennard, D. G. Watson, L. Brammer, A. G. Orpen, R. Taylor, *J. Chem. Soc., Perkin Trans. 2* **1987**, S1–S19.
[34] F. H. Allen, *Acta Crystallogr., Sect. B: Struct. Sci.* **2002**, *58*, 380–388.

Received: August 22, 2007
Published Online: December 20, 2007

